ACS OMEGA

http://pubs.acs.org/journal/acsodf

Article

Adsorption and Photocatalytic Degradation of Methylene Blue on TiO_2 Thin Films Impregnated with Anderson-Evans Al-Polyoxometalates: Experimental and DFT Study

Freider Duran, Carlos Diaz-Uribe, William Vallejo,* Amner Muñoz-Acevedo, Eduardo Schott, and Ximena Zarate

Cite This: *ACS Omega* 2023, 8, 27284−27292

Read Online

ACCESS | Metrics & More | Article Recommendations | Supporting Information

ABSTRACT: In this work, we fabricated a TiO_2 thin film, and the same film was modified with an Anderson aluminum polyoxometalate (TiO_2-AlPOM). Physical−chemical characterization of the catalysts showed a significant change in morphological and optical properties of the TiO_2 thin films after surface modification. We applied the kinetic and isothermal models to the methylene blue (MB) adsorption process on both catalysts. The pseudo-second order model was the best fitting model for the kinetic results; *qe* (mg/g) was 11.9 for TiO_2 thin films and 14.6 for TiO_2-AlPOM thin films, and k_2 (g mg^{-1} min^{-1}) was 16.3×10^{-2} for TiO_2 thin films and 28.2×10^{-2} for TiO_2-AlPOM thin films. Furthermore, the Freundlich model was suitable to describe the isothermal behavior of TiO_2, K_F (5.42 mg/g), and $1/n$ (0.312). The kinetics of photocatalytic degradation was fitted using the Langmuir−Hinshelwood model; k_{ap} was 7×10^{-4} min^{-1} for TiO_2 and 13×10^{-4} min^{-1} for TiO_2-AlPOM. The comparative study showed that TiO_2 thin films reach a 19.6% MB degradation under UV irradiation and 9.1% MB adsorption, while the TiO_2-AlPOM thin films reach a 32.6% MB degradation and 12.2% MB adsorption on their surface. The surface modification improves the morphological, optical, and photocatalytic properties of the thin films. Finally, the DFT study supports all the previously shown results.

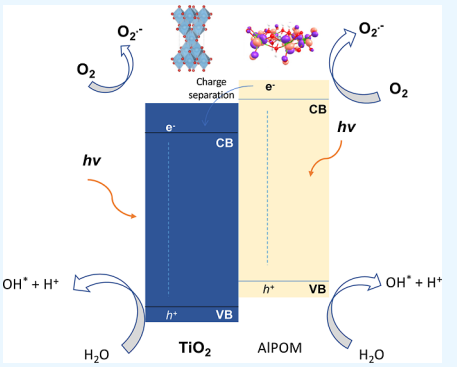

1. INTRODUCTION

In the last few decades, the emerging pollutants have become a relevant issue, as they can affect the environmental quality and the public health.[1] They represent a wide variety of chemical compounds [e.g., pharmaceuticals, hormones and steroids, disinfection by-products, hygiene and personal care products, surfactants, flame retardants, industrial compounds, agrochemicals (pesticides, fertilizers, and growth agents), microplastics, and dyes].[2,3] These compounds are chemically and physically stable enough to withstand conventional treatment processes and are not properly degraded in treatment plants.[4] Heterogeneous photocatalysis (HP) has demonstrated its potential for treatment of various emerging pollutants.[5,6] HP can convert solar energy into chemical energy under the action of photocatalysts; this technique provides new ideas for the development of traditional catalysis. Nowadays, titanium dioxide (TiO_2) has become the main photocatalyst that is studied for the development of environmental applications.[7,8] However, TiO_2 has two drawbacks: (i) high band gap energy value (3.2 eV, active only under UV irradiation) and (ii) low quantum efficiency in charge-carrier generation.[9] Various methods have been reported to solve these issues [e.g., metal doping,[10] quantum dots,[11] sensitization with a smaller band gap semiconductors,[12] surface plasmon resonance,[13] sensitization with natural and synthetic dyes,[14,15] and surface modification of TiO_2 with inorganic compounds such as polyoxometalates (POMs).[16] Among these strategies, fabrication of hybrid materials TiO_2-POMs has been given great attention due to the photophysical properties of POMs.[17,18] These compounds are metal−oxygen anion nanoclusters formed primarily by the condensation of tungstates or molybdates with or without the involvement of a variety of other elements.[19] Among POMs, there are three main structures, which are known as Keggin, Anderson-Evans, and Wells−Dawson. The Keggin-type structure has a general formula $X_{n+1}M_{12}O_{40}^{(8-n)}$ (M/X = 12); they are the most studied compounds even for catalytic applications, due to their facilities in the synthesis process, relatively high thermal stability, and redox and acidic properties.[20] Knoth et al. reported the first case of Ti-substituted Keggin-type monomeric $[TiW_{11}PO_{40}]^{5-}$ polyoxoanion cluster.[21] The Wells−Dawson-type structure has a general formula of

Received: April 18, 2023
Accepted: June 1, 2023
Published: July 20, 2023

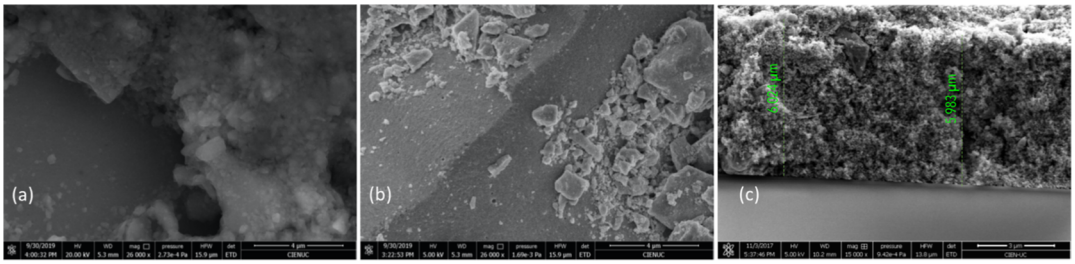

Figure 1. SEM images: (a) TiO_2 thin films (×26,000), (b) TiO_2-AlPOM (×26,000), and (c) cross-section SEM ×15,000 image of the TiO_2 films.

$X_{2n}M_{18}O_{62}^{(2n-16)}$ (X is P^{5+}, S^{6+}, and As^{5+}; M can be W^{6+} or Mo^{+6}) (m/x = 9). The Wells−Dawson-type POMs have reported photocatalytic activity; Fan et al. reported the efficient photocatalytic degradation of different dyes on (P_2W_{18}) modified by a Ag complex.[22] The Anderson-type POMs have a general formula of $H_i(XO_6)M_{18}^{(n-)}$ (M/X = 6); they have a plane structure consisting of a central XO_6 octahedral structural unit surrounded by six edge-sharing MO_6 octahedral structural units; these compounds have a great variety of the central heteroatom, which has significant impacts on their electronic and catalytic properties.[23] Qin et. at. reported the photocatalytic activity of organic−inorganic hybrid Anderson-type POMs under visible-light irradiation.[24] Wang et al. synthesized novel Anderson-type POMs based on metal−organic frameworks.[25] Because POMs can act as mediators in the dynamics of photocatalytic electronic transfer from the conduction band of TiO_2, they can be used to form composites with other semiconductors.[26] Diaz-Uribe et al. reported the synergic effect of Anderson-type Cr-POM and Zn-POM anchored to TiO_2 thin films in photocatalytic degradation of methylene blue (MB).[27] Recently, our research group reported the synergic effect of Anderson-type (ZnPOM and CuPOM) and a porphyrin anchored to TiO_2 thin films in photocatalytic degradation of MB.[28]

In this article, we modified TiO_2 thin films with Anderson-type POM aluminum and studied physical adsorption and photocatalytic degradation of MB under UV irradiation. Finally, by means of DFT modeling, the comparison with the previously reported POMs supported over TiO_2 was made, showing a reasonable explanation of the performance observed for the AlPOM reported herein.

2. EXPERIMENTAL SECTION

2.1. Synthesis of the Catalysts and Thin Film Deposition. The aluminum Anderson-POMs were synthesized as ammoniacal salts with general chemical formula $(NH_4)_3[AlMo_6O_{24}H_6]^{-3}$*$4H_2O$. The POM was prepared through the precipitation reaction between the precursor $(NH4)_6Mo_7O_{24}{\cdot}4H_2O$ (Merck, 99%) and $Al(NO_3)_3{\cdot}9H_2O$ (Merck, ≥99) according to procedure reported by Lee.[29] The synthesized POMs correspond to $(NH_4)_3[AlMo_6O_{24}H_6]{\cdot}4H_2O$ called AlPOM. The TiO_2 films were deposited on soda lime glass by the Doctor Blade method, and TiO_2−Degussa powder (P25) was used as reagent; the details of the procedure are provided in a previous report.[30,31] The TiO_2 thin films were immersed in a solution of POMs (10 mg/L) for 24 h at room temperature and under constant stirring. Finally, the films were washed with water and dried at 90 °C during 12 h.

2.2. Characterization of the Thin Films. The thin films' optical properties were determined by diffuse reflectance using a Lambda 4 PerkinElmer spectrometer equipped with an integrating sphere. Morphology and elemental surface assays were carried out by scanning electron microscopy and energy-dispersive X-ray spectroscopy (SEM−EDX), and the samples were analyzed using the SEM instrument model QUANTA FEG 650 with operation at an acceleration potential of 25.0 kV. For chemical content assay, we used detector EDAX APOLO 126.1 eV (Mn Kα) and the software EDX Genesis to generate the semi-quantitative information.

2.3. Adsorption Study. We study the kinetic and isothermal adsorption of MB on the thin films fabricated in this work. First, the thin films were immersed in a solution of MB (100 mL; 10 mg/L) (Merck, ≥95%) contained in a batch glass reactor provided with an air bubbling system (0.5 L/min). The reactor was stored in the dark to study the MB adsorption process on the films. An aliquot was extracted at time zero and every 5 min thereafter to track the kinetics of the process and to determine the adsorption−desorption equilibrium time. The process was repeated with different MB concentrations (20, 30, 40, 50, and 60 mg/L). The MB concentration of each aliquot was determined by spectrophotometry at 665 nm (Thermo Scientific Evolution 220 spectrophotometer) using the Lambert−Beer law with a calibration curve (R^2 = 0.996). As a previous step to the photocatalytic degradation, the adsorption of contaminant species on the surface of the photocatalyst (sorption/desorption equilibrium) is a very important step of the process; however, this step is not commonly reported in photocatalytic studies. In this work, we studied the adsorption behavior of BM onto both materials fabricated as a previous step to the photocatalytic degradation by using Langmuir, Freundlich, Temkin, and Dubinin−Radushkevich isothermal models. All the details of this section are given in Supporting Information (Section S1).

2.4. Photocatalytic Study. Once the adsorption−desorption equilibrium was reached, the reactor with the MB solution (100 mL; 10 mg/L) and the film was irradiated with an UV tubular lamp manufactured by PHILIPS (arc length 161 mm, tube diameter 16 mm, 7 W, 15 $\mu W/cm^2$ at 1 m, emission maximum of 260 nm) during 5 h, and every 20 min a sample was extracted to monitor the MB degradation. In the study, the photocatalytic degradation of MB under UV and vis irradiation was fitted with Langmuir−Hinshelwood according to[32]

$$[MB]_t = [MB]_o\, e^{-k_{ap}(t)} \quad (1)$$

where $[MB]_t$ is the MB concentration as function of light irradiation, (t) is the irradiation time, and k_{ap} is the apparent reaction rate constant (min^{-1}).

2.5. DFT Study. Density functional theory (DFT) calculations were carried out with the Amsterdam Density Functional package (ADF 2019.01)[33] at the relativistic level

https://doi.org/10.1021/acsomega.3c02657
ACS Omega 2023, 8, 27284−27292

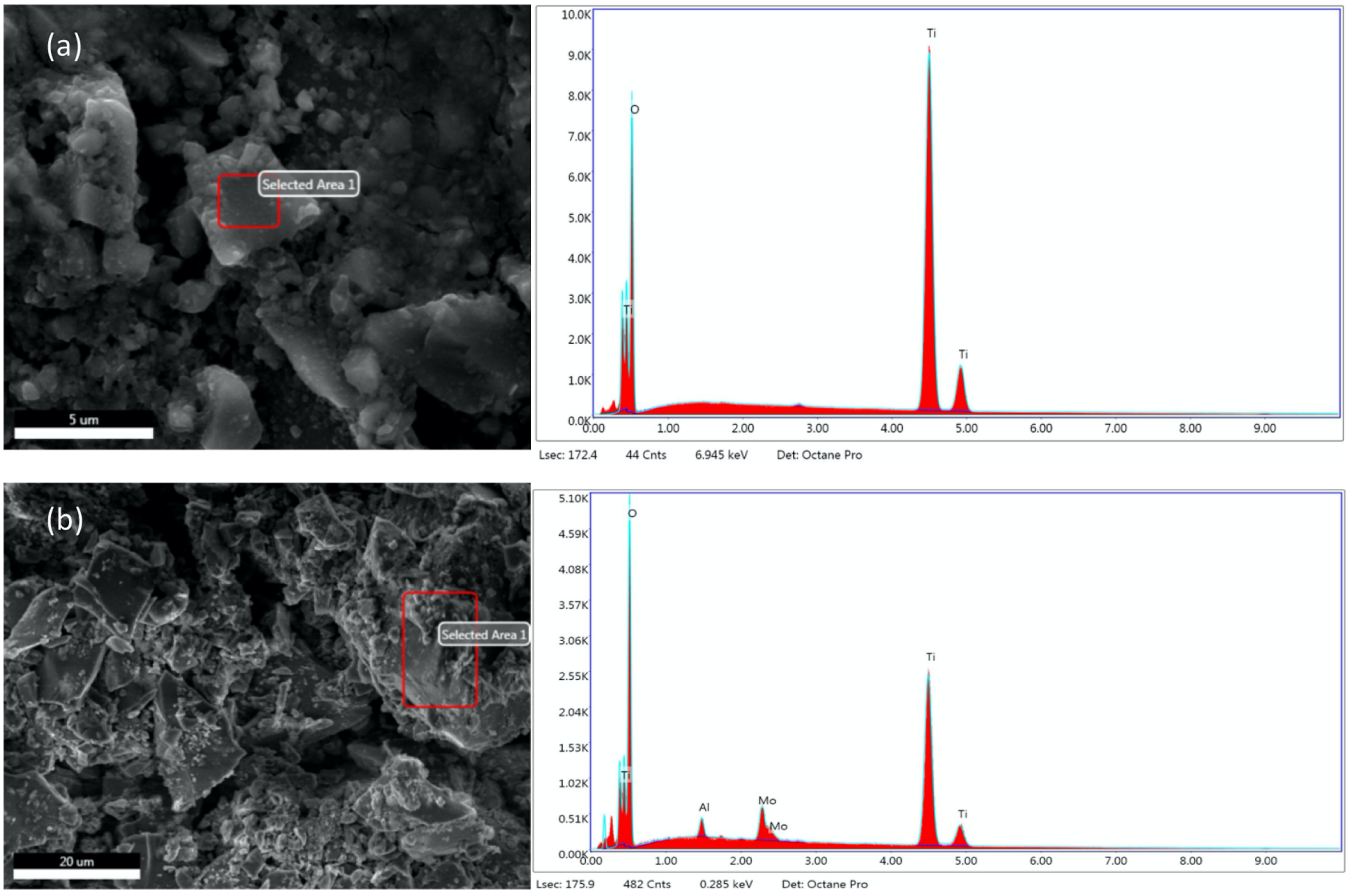

Figure 2. EDX images: (a) TiO_2 thin films (×26,000) and (b) TiO_2-AlPOM (×26,000).

including the zeroth order regular approximation Hamiltonian with the scalar corrections.[33,34] Single polarized uncontracted type IV basis sets using triple-ζ accuracy sets of slater type orbitals were employed.[35] The generalized gradient approximation method was used for the optimizations via analytical energy gradient techniques using the nonlocal exchange and correlation corrections within the PBE functional.[36] Solvent effects were included using COSMO with water as solvent.[37] Using the bonding energy decomposition analysis, proposed by Morokuma−Ziegler,[33,38,39] the interaction energy, ΔE_{int}, was dissected into the $\Delta E_{elec.} + \Delta E_{Pauli} + \Delta E_{orb}$ components. (i) $\Delta E_{elec.}$ is the electrostatic component, calculated by superposition of the unperturbed fragment densities of the molecular geometry, corresponding to the classical electrostatic effects due to the attractive and repulsive forces; (ii) ΔE_{Pauli} represents the repulsive interactions between the fragments because two electrons with the same spin cannot occupy the same region in the space; and (iii) $\Delta E_{orb.}$ is the stabilizing orbital interaction term.[40]

3. RESULTS AND DISCUSSION

3.1. Morphological Characterization. Figure 1 shows the SEM image for TiO_2 and TiO_2-AlPOM thin films. Images show agglomeration in the form of particles on the TiO_2 thin films with varying sizes. Holes on the TiO_2 film could be observed; this result could be attributed to the process of homogenization of the catalyst slurry during the Doctor Blade deposition of the films.[41]

The semiconductor industry has developed different methods for thin film depositions (e.g., chemical vapor deposition, sputtering, thermal evaporation, atomic layer deposition, sol−gel, chemical bath deposition, and Doctor Blade).[42] Among the physical and chemical methods of thin film deposition, the Doctor Blade process is inexpensive and technically suitable one (e.g., temperature and pressure requirements).[43] The Doctor Blade technique deposits thicker films by increasing deposition speed affecting final morphological properties of the coatings.[44] TiO_2-AlPOM film has a more heterogeneous surface in terms of particle size and distribution compared with TiO_2 thin films. This behavior is according to previous reports about TiO_2 surface modification with POMs. Sun et al. reported particulate aggregation of POMs after electrodeposition of PW_{12} polyanions on the TiO_2 surface.[45] Figure 1c shows the cross-section SEM ×15,000 image of the TiO_2 film; the SEM images indicate that the thickness of the TiO_2 thin films was near ∼6.0 μm (average 6 points). Figure 2 shows the EDX assay for TiO_2 and TiO_2-AlPOM thin films, and Table 1 lists the elemental composition of the thin films.

Table 1. Elemental Composition Analysis for TiO_2 and TiO_2-AlPOM Thin Films

film[a]	% Ti	% O	% Mo	% Al
TiO_2	33.32	66.68		
TiO_2-AlPOM	31.53	66.06	2.05	0.36

[a]The film composition was obtained with EDX characterization results.

https://doi.org/10.1021/acsomega.3c02657
ACS Omega 2023, 8, 27284−27292

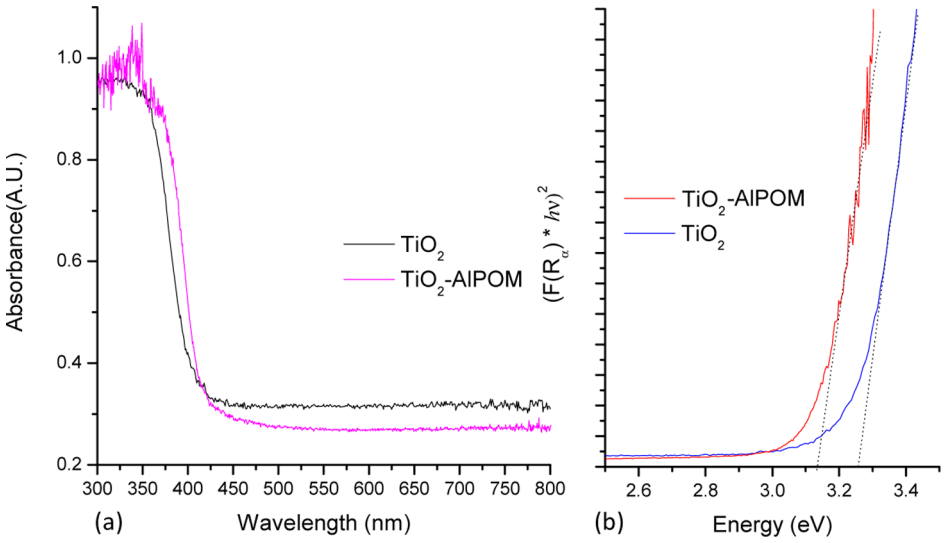

Figure 3. (a) Thin film diffuse reflectance spectra and (b) Kubelka−Munk plots.

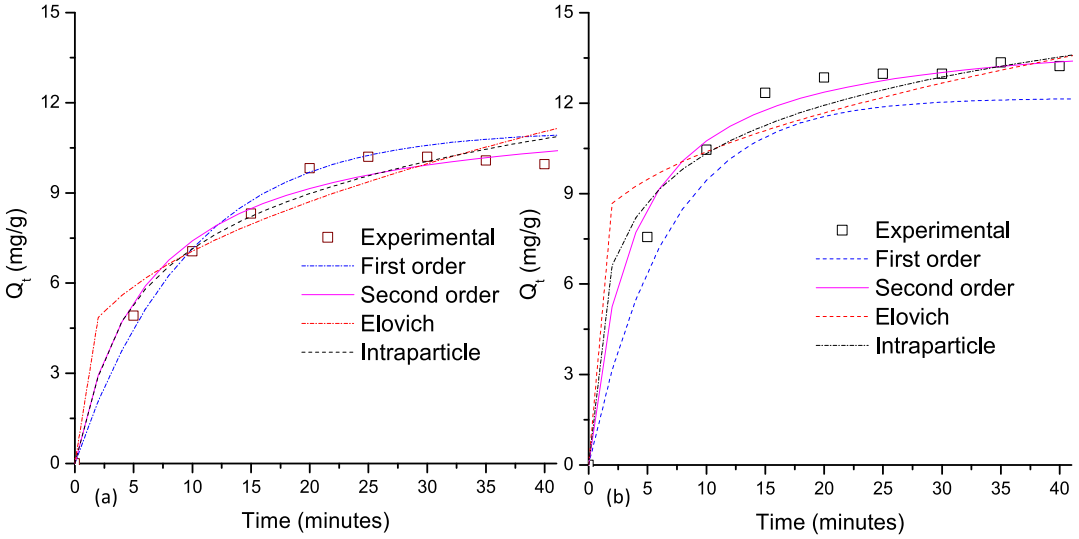

Figure 4. Kinetic results and model fitting for adsorption of MB on: (a) TiO_2. (b) TiO_2-AlPOM thin films.

Table 2. Kinetic Values Calculated for MB Sorption Onto Films

thin film/model[a]	1st order	2nd order	Elovich	intraparticle
TiO_2	qe(mg g^{-1}) = 11.1	qe(mg/g) = 11.9	α (mg g^{-1} min^{-1}) × 10^{-2}= 56.8	C (mg/g) = 3.1
	k_1 (min^{-1}) × 10^{-3}= 104	K_2 (g mg^{-1} min^{-1}) × 10^{-3}= 163	β (g mg^{-1}) = 2.63	k_{id} (g $mg^{-1}min^{-1/2}$) = 1.3
	R^2 = 0.960	R^2 = 0.987	R^2 = 0.918	R^2 = 0.830
	ARE (%) = 4.1	ARE (%) = 3.0	ARE (%) = 8.5	ARE (%) = 15.3
TiO_2-AlPOM	qe(mg g^{-1}) = 12.1	qe(mg/g) = 14.6	α (mg g^{-1} min^{-1}) × 10^{-2}= 376	C (mg/g) = 7.3
	k_1 (min^{-1}) × 10^{-3}= 150	K_2 (g $mg^{-1}min^{-1}$) × 10^{-3}= 282	β (g mg^{-1}) = 2.31	k_{id} (g $mg^{-1}min^{-1/2}$) = 0.98
	R^2 = 0.971	R^2 = 0.998	R^2 = 0.841	R^2 = 0.841
	ARE (%) = 6.7	ARE (%) = 2.3	ARE (%) = 7.7	ARE (%) = 29

[a]Parameters obtained from the fitting data of Figure 4.

3.2. Optical Characterization. Figure 3a shows the diffuse reflectance spectra for TiO_2 and TiO_2-AlPOM thin films. The TiO_2 thin films spectra show strong absorption at wavelength higher than 380 nm; this is according to its band gap value and previous reports about TiO_2 optical properties. The TiO_2-AlPOM thin film spectra show that surface modification affects the optical properties of thin films. Figure 3a shows a red shift of the absorption edge of TiO_2-AlPOM thin films compared to bare TiO_2. This result is associated with the charge transfer of the Mo(VI) in an octahedral environment. In these structures, the Mo atoms have the highest oxidation state, and Mo(VI) with an electronic configuration d_0 and the ligand to metal charge transfer (LMCT) O → Mo could be present.[46] The interaction of the TiO_2 electronic bands with the POM HOMO−LUMO orbitals allow POMs to act as electron acceptors reducing electron-hole recombination

https://doi.org/10.1021/acsomega.3c02657
ACS Omega 2023, 8, 27284−27292

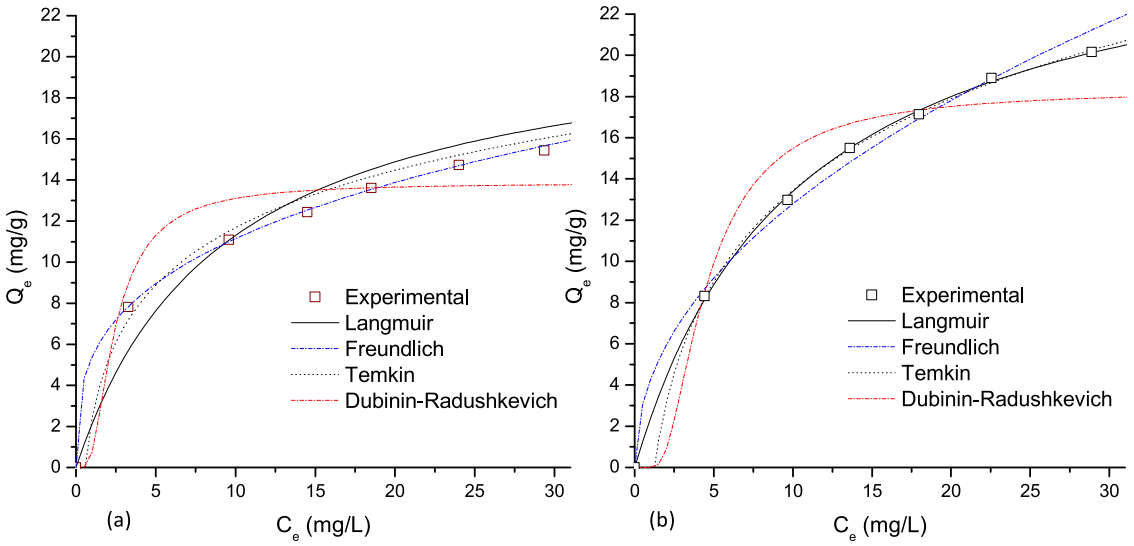

Figure 5. Isothermal results and model fitting for adsorption of MB on: (a) TiO_2. (b) TiO_2-AlPOM thin films.

Table 3. Isotherm Models Fitting Results for MB Isotherm Adsorption on Catalysts

thin film/model[a]	Freundlich	Langmuir	Temkin	Dubinin−Radushkevich
TiO_2	K_F (mg/g)/(mg/L)^n = 5.4	q_m (mg/g) = 21.8	B_T = 42.48	β (mol^2 kJ^{-2}) × 10^{-6}= 1.0
	$1/n$ = 0.312	K_L (L/mg) = 0.109	A_T = 2.40	q_m (mg/g) = 13.6
	R^2 = 0.999	R^2 = 0.986	R^2 = 0.918	R^2 = 0.873
	ARE (%) = 1.0	ARE (%) = 7.5	ARE (%) = 3.8	ARE (%) = 10.8
TiO_2-AlPOM	K_F (mg/g)/(mg/L)^n = 4.3	q_m (mg/g) = 27.4	B_T = 6.41	β (mol^2 kJ^{-2}) × 10^{-6}= 3.0
	$1/n$ = 0.477	K_L (L/mg) = 0.100	A_T = 1.22	q_m (mg/g) = 18.3
	R^2 = 0.986	R^2 = 0.999	R^2 = 0.996	R^2 = 0.910
	ARE (%) = 3.0	ARE (%) = 1.1	ARE (%) = 1.7	ARE (%) = 7.9

[a]Parameters obtained from the fitting data of Figure 5.

of photo-generated electrons by TiO_2.[19] Guo et al., deposited Keggin-type POMs on mesoporous-TiO_2 nanoparticles for photocatalytic degradation of methyl orange.[47] They reported a significant red shift to the visible region UV−vis spectra of the light absorption of TiO_2 after POM deposition. The band gap energy value was determined using the Kubelka−Munk remission function.[48] Figure 3b shows the plot $(F(R_\infty)hv)^{1/2}$ vs (hv) for the spectra shown in Figure 3a, and Figure 3b shows band gap energy estimation for films. The estimated bad gap for materials was 3.24 eV for TiO_2 thin films and 3.12 eV for TiO_2-AlPOM thin films. The TiO_2 thin films' band gap energy value is in agreement with the reports in literature, which verifies that TiO_2 is active only under UV irradiation.[49] The change in the optical properties of TiO_2-AlPOM thin films is due to the interactions of the TiO_2 electronic bands with the AlPOM HOMO−LUMO orbitals.[27]

3.3. Adsorption Study. *3.3.1. Kinetic Study.* Figure 4 shows the MB adsorption kinetics onto films applying the four theoretical fitting models, and Table 2 shows all the kinetic parameters. The percentage of MB adsorbed on catalysts was 9.96 and 13.1 mg/g for TiO_2 and TiO_2-AlPOM, respectively. The results show an increase in the percentage of MB adsorbed on the surface catalyst after surface modification; this result could be associated to the morphological and ionic nature of POMs: (i) after POM adsorption on the TiO_2 surface, the surface was more heterogeneous in terms of both particle size and distribution comparing with TiO_2 thin films (Section 3.1.) affecting the MB adsorption. (ii) The Anderson-type POMs are of an anionic nature, so there is a higher attraction between the POMs and MB, resulting in a better adsorption on the films.[28] Comparing fitting results (Table 2), the pseudo-second order model showed the best fitting regression values among all models (higher R^2 and lower ARE values). In this model, the effective electrostatic interactions play an important role in adsorption. The results suggest that chemisorption could be the dominant interaction during the adsorption of MB onto both thin films.[32,50]

3.3.2. Isothermal Study. Figure 5 shows the isotherm fitting results for MB adsorption on thin films. Table 3 lists the isotherm parameters for all models. According to results listed in Table 3, the Freundlich model was the best fitting model (higher R^2 and smaller ARE) for TiO_2 thin films. This model is described as a multilayer with a heterogeneous surface. In this model, the adsorption heat and affinities between adsorbent and adsorbates are not uniformly distributed on the heterogeneous surface. Furthermore, this model is commonly utilized in heterogeneous systems (e.g., active carbon, zeolites, and some semiconductors).[51] This model agrees with the morphological results. Furthermore, the Langmuir and Temkin models were the best fitting models for TiO_2-AlPOM thin films (ARE and R^2 values are very close for both models). Langmuir isotherm accounts for the surface coverage by balancing the relative rates of adsorption and desorption (dynamic equilibrium). The Temkin model takes into account the effects of indirect adsorbate/adsorbate interactions on the adsorption process.[52] In our case, in heterogeneous surfaces, it is possible that more than one model fits the experimental data, which would mean that several types of adsorption processes

https://doi.org/10.1021/acsomega.3c02657
ACS Omega 2023, 8, 27284−27292

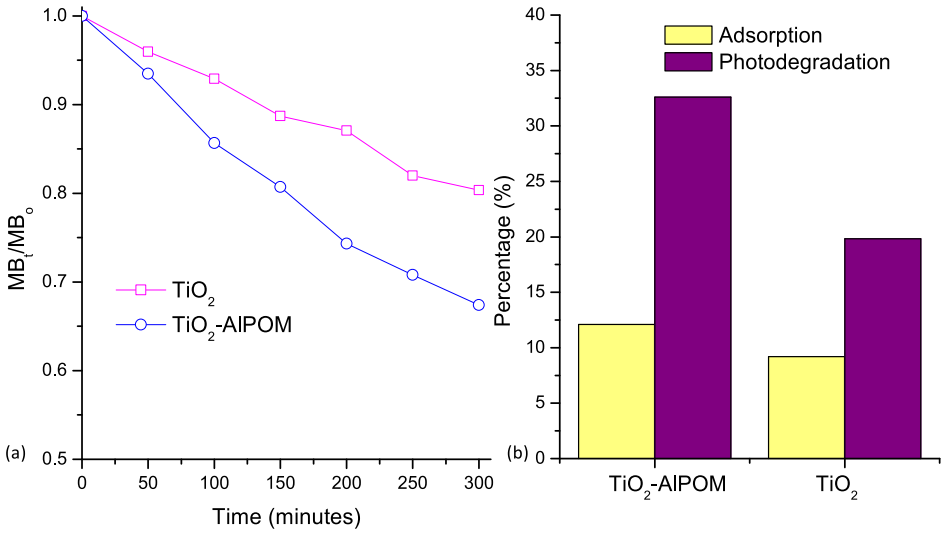

Figure 6. (a) MB photocatalytic degradation under UV irradiation onto catalysts. (b) Comparison between TiO_2 and TiO_2-AlPOM thins films in photocatalytic and adsorption studies.

can be present during the adsorption MB on catalysts. This would mean that several types of adsorption processes participate during the MB adsorption process. According to both kinetic and isothermal results, chemisorption could be the dominant interaction during the MB adsorption onto the catalyst, where effective electrostatic interactions play an important role in adsorption.

3.4. Photocatalytic Study. Figure 6a shows the MB concentration as a function of UV-irradiation time onto catalysts. The results indicate that TiO_2 thin films reach a 19.6% of MB degradation under UV irradiation and TiO_2-AlPOM thin films reach a 32.6% MB degradation value. These results are associated with the effect of AlPOM on morphological, optical, and surface properties; besides, the redox properties of POMs can reduce the recombination rates on TiO_2 thin films. The photocatalytic data were fitted using the Langmuir−Hinshelwood model (eq 1). Results indicated that k_{ap} was 7×10^{-4} min^{-1} for TiO_2 and 13×10^{-4} min^{-1} for TiO_2-AlPOM. Comparing these results, the TiO_2-AlPOM thin films were 1.85 faster than TiO_2 thin films in MB photodegradation. After modification, POMs can act as a scavenger, gathering photogenerated electrons from the TiO_2 and delaying the recombination of charge carriers.[19,53] The AlPOM interaction with TiO_2 changes morphological, optical, and adsorption catalyst properties, generating a synergic effect in the photocatalytic activity. Comparing the herein obtained results with previous reports, k_{ap} for TiO_2-AlPOM is smaller than the k_{ap} value reported for TiO_2 thin films modified with Cr-POM (60×10^{-3} min^{-1}).[54] In this case, the electronic configuration of Al inside the POM does not possess free "d" orbital compared with Cr that has free "d" orbital to reduce de recombination rates. Figure 6b shows the comparison between TiO_2 and TiO_2-AlPOM thins films in photocatalytic and adsorption studies.

The comparative study showed that TiO_2 thin films reach a 19.6% MB degradation under UV irradiation and 9.1% MB adsorption, while the TiO_2-AlPOM thin films reach a 32.6% MB degradation and 12.1% MB adsorption on their surface. In combination (adsorption and photodegradation), TiO_2 thin films reach 27.1% MB remotion and TiO_2-AlPOM thin films reach 44.6% MB removal. The previous stage to the photocatalytic degradation is more efficient to anchor more MB on the catalyst surface to TiO_2-AlPOM than to TiO_2 thin films, which is due to anionic properties of the POM. Furthermore, POMs can be photocatalytic active under UV irradiation, which could make the POM a generator of reactive species contributing to the degradation of the model pollutant.[55] POMs have an electronic structure similar to the semiconductors (e.g., conduction band and valence band).[23,53] Figure S1 shows the UV−vis absorption spectra of AlPOM in an aqueous solution. Figure S1 shows two absorption bands close to 208 and 228 nm; the transitions are associated with ligand to metal charge transfer (O → Mo); these charge transfers have been reported at wavelengths between 200 and 350 nm.[46] This photoexcitation of the POMs can be applied in HP.[56] In our case, the composite structure TiO_2-AlPOM improved the photocatalytic yield compared with the bare TiO_2 thin films due to three reasons: (i) AlPOM can generate reactive oxygen species (ROS) in the same way that TiO_2 can, which increases the charge carriers available to photodegradation; (ii) the heterostructure of composite TiO_2-AlPOM assists the charge separation, reducing the recombination process; and (iii) the surface area of the semiconductor can increase after POM modification.[19,57] After charge pairs generation (by TiO_2 and/or AlPOM), the ROS can be yielded on the composite surface and MB degradation starts. Figure 7 shows the ROS process for TiO_2-AlPOM thin films.

3.5. DFT Study. There is a previous study on the POM family with Co, Cr, and Ni. It was shown that the best catalyst for the photocatalytic MB degradation among those three compounds adsorbed over TiO_2 was Cr.[54] This was due to the presence of unpaired electrons due to the oxidation state of the central metallic atom. Furthermore, it was shown that the more spin density is located over the central metallic atom, the better the catalyst is. This situation was outstanding for the Cr-POM, which showed the large unpaired spin between all the former studied derivatives. Thus, when there is a large participation of the surrounding metallic atoms, the catalyst is worse. In this report, as can be observed in Figure 8, the geometry of the POM does not get affected by the inclusion of the Al^{3+} at the center of the POM. The Frontier molecular orbitals (FMO) are mostly located over the surrounding atoms of the Anderson

https://doi.org/10.1021/acsomega.3c02657
ACS Omega 2023, 8, 27284−27292

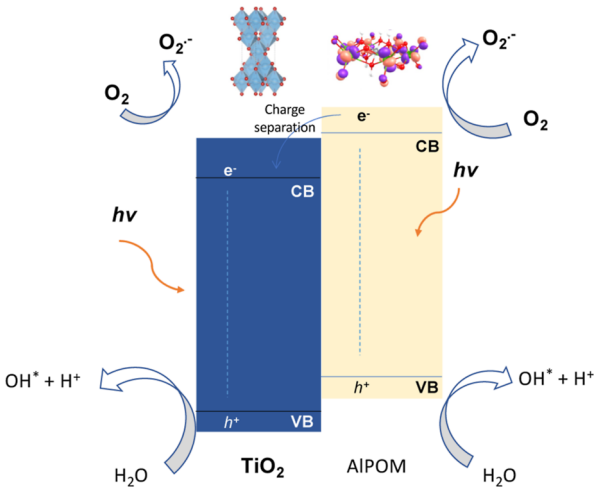

Figure 7. (a) Photocatalytic scheme of TiO_2-AlPOM thins films fabricated in this work. Inset: CB is the conduction band and VB is the valence band.

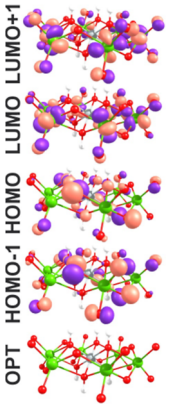

Figure 8. FMOs for AlPOM synthesized.

POM. Furthermore, there is no spin density, as the Al^{3+} corresponds to a close shell atom, which does not show any unpaired electrons. In terms of stabilization energy, the reported compound does show a stability similar to the best catalyst reported before (−92.4 eV). This stability can be related to the long-lasting stability of the studied molecule in the reaction procedure. Finally, 71% of the observed stabilization energy corresponds to electrostatic interaction inside the molecule and between the central metallic (−69.1 eV) Al^{3+} atom and the surrounding structure, whereas the orbital energy represents only 29%(−28.2 eV). This observation is similar to the previous report.

4. CONCLUSIONS

In this work, we modified TiO_2 thin films with AlPOM. The catalysts were characterized by optical and morphological techniques. We studied the effect of AlPOM on TiO_2 thin films properties for adsorption and photocatalytic degradation of MB. After AlPOM modification, the thin films' adsorption capacity and photocatalytic activity improved. These results were associated with a synergic effect between Al-POM and TiO_2. After POM modification, the adsorption capacity changed from 9.1 to 12.2%, and the photocatalytic efficiency changed from 19.6 to 32.6%; the best results were obtained using TiO_2-AlPOM thin films. Results show that several types of adsorption processes participate during the MB adsorption process, and results indicated that the adsorption process is an important step prior to photocatalytic degradation (remove an important amount of the pollutant). Furthermore, the TiO_2-AlPOM thin films were 1.85 faster than TiO_2 thin films in MB photodegradation. DFT results showed that the geometry of the POM does not get affected by the inclusion of the Al^{3+} at the center of the POM generating long-lasting stability for adsorption and photocatalytic application.

■ ASSOCIATED CONTENT

Supporting Information

The Supporting Information is available free of charge at https://pubs.acs.org/doi/10.1021/acsomega.3c02657.

Isothermal and kinetic models and UV−vis absorption spectra of synthesized AlPOM (PDF)

■ AUTHOR INFORMATION

Corresponding Author

William Vallejo − *Grupo de Investigación en Fotoquímica y Fotobiología. Programa de Química. Facultad de Ciencias Básicas, Universidad del Atlántico, Puerto Colombia 81007, Colombia;* orcid.org/0000-0002-6661-545X; Email: williamvallejo@mail.uniatlantico.edu.co

Authors

Freider Duran − *Grupo de Investigación en Fotoquímica y Fotobiología. Programa de Química. Facultad de Ciencias Básicas, Universidad del Atlántico, Puerto Colombia 81007, Colombia*

Carlos Diaz-Uribe − *Grupo de Investigación en Fotoquímica y Fotobiología. Programa de Química. Facultad de Ciencias Básicas, Universidad del Atlántico, Puerto Colombia 81007, Colombia*

Amner Muñoz-Acevedo − *Grupo de Investigación en Química y Biología, Universidad del Norte, Puerto Colombia 81007, Colombia*

Eduardo Schott − *Departamento de Química Inorgánica, Facultad de Química y Farmacia, Centro de Energía UC, Centro de Investigación en Nanotecnología y Materiales Avanzados CIEN-UC, Pontificia Universidad Católica de Chile, Santiago 4860, Chile; Millenium Nuclei on Catalytic Processes towards Sustainable Chemistry (CSC), Concepción 4030000, Chile*

Ximena Zarate − *Instituto de Ciencias Químicas Aplicadas, Facultad de Ingeniería, Universidad Autónoma de Chile, Santiago 7500912, Chile*

Complete contact information is available at: https://pubs.acs.org/10.1021/acsomega.3c02657

Notes

The authors declare no competing financial interest.

■ ACKNOWLEDGMENTS

W.V. and C.D.-U. thank Universidad del Atlántico, Ministry of Economy, Development and Tourism-Chile, grant Nuclei on Catalytic Processes towards Sustainable Chemistry (CSC) ANID-NCN2021_090. ANID/FONDAP/1522A0006. ACT210057. FONDEQUIP EQM 15010. A. M.-A. thanks the Vicerrectoría de Investigaciones of the Universidad del Norte for financial support for the of article processing charge.

REFERENCES

(1) Martín-Pozo, L.; de Alarcón-Gómez, B.; Rodríguez-Gómez, R.; García-Córcoles, M. T.; Çipa, M.; Zafra-Gómez, A. Analytical Methods for the Determination of Emerging Contaminants in Sewage Sludge Samples. A Review. *Talanta* **2019**, *192*, 508−533.

(2) Ramírez-Malule, H.; Quiñones-Murillo, D. H.; Manotas-Duque, D. Emerging Contaminants as Global Environmental Hazards. A Bibliometric Analysis. *Emerging Contam.* **2020**, *6*, 179−193.

(3) Lodeiro, C.; Capelo, J. L.; Oliveira, E.; Lodeiro, J. F. New Toxic Emerging Contaminants: Beyond the Toxicological Effects. *Environ. Sci. Pollut. Res.* **2019**, *26*, 1−4.

(4) Liu, B.; Zhang, S. gen; Chang, C. C. Emerging Pollutants-Part II: Treatment. *Water Environ. Res.* **2019**, *91*, 1390−1401.

(5) Aoudj, S.; Drouiche, N.; Khelifa, A. Emerging Contaminants Remediation by Heterogeneous Photocatalysis. In *Emerging and Nanomaterial Contaminants in Wastewater: Advanced Treatment Technologies*; Elsevier, 2019; pp 245−275. DOI: 10.1016/B978-0-12-814673-6.00009-7.

(6) Antonopoulou, M.; Kosma, C.; Albanis, T.; Konstantinou, I. An Overview of Homogeneous and Heterogeneous Photocatalysis Applications for the Removal of Pharmaceutical Compounds from Real or Synthetic Hospital Wastewaters under Lab or Pilot Scale. *Sci. Total Environ.* **2021**, *765*, 144163.

(7) Sharma, M.; Yadav, A.; Mandal, M. K.; Dubey, K. K. TiO2 Based Photocatalysis: A Valuable Approach for the Removal of Pharmaceuticals from Aquatic Environment. *Int. J. Environ. Sci. Technol.* **2022**, *20*, 4569−4584.

(8) He, F.; Jeon, W.; Choi, W. Photocatalytic Air Purification Mimicking the Self-Cleaning Process of the Atmosphere. *Nat. Commun.* **2021**, *12*, 2528.

(9) Danish, M.; Ambreen, S.; Chauhan, A.; Pandey, A. Optimization and Comparative Evaluation of Optical and Photocatalytic Properties of TiO2 Thin Films Prepared via Sol−Gel Method. *J. Saudi Chem. Soc.* **2015**, *19*, 557−562.

(10) Sudrajat, H.; Hartuti, S.; Babel, S. Mechanistic Understanding of the Increased Photoactivity of TiO2 Nanosheets upon Tantalum Doping. *Phys. Chem. Chem. Phys.* **2022**, *24*, 995−1006.

(11) Yashwanth, H. J.; Rondiya, S. R.; Dzade, N. Y.; Hoye, R. L. Z.; Choudhary, R. J.; Phase, D. M.; Dhole, S. D.; Hareesh, K. Improved Photocatalytic Activity of TiO2 Nanoparticles through Nitrogen and Phosphorus Co-Doped Carbon Quantum Dots: An Experimental and Theoretical Study. *Phys. Chem. Chem. Phys.* **2022**, *24*, 15271−15279.

(12) Rahimi, N.; Pax, R. A.; Gray, E. M. A. Review of Functional Titanium Oxides. I: TiO2 and Its Modifications. *Prog. Solid State Chem.* **2016**, *44*, 86−105.

(13) Shuang, S.; Lv, R.; Xie, Z.; Zhang, Z. Surface Plasmon Enhanced Photocatalysis of Au/Pt-Decorated TiO2 Nanopillar Arrays. *Sci. Rep.* **2016**, *6*, 26670.

(14) Diaz-Angulo, J.; Gomez-Bonilla, I.; Jimenez-Tohapanta, C.; Mueses, M.; Pinzon, M.; Machuca-Martinez, F. Visible-Light Activation of TiO2 by Dye-Sensitization for Degradation of Pharmaceutical Compounds. *Photochem. Photobiol. Sci.* **2019**, *18*, 897−904.

(15) Vallejo, W.; Rueda, A.; Díaz-Uribe, C.; Grande, C.; Quintana, P. Photocatalytic Activity of Graphene Oxide−TiO2 Thin Films Sensitized by Natural Dyes Extracted from Bactris Guineensis. *R. Soc. Open Sci.* **2019**, *6*, 181824.

(16) Fotiou, T.; Triantis, T. M.; Kaloudis, T.; Papaconstantinou, E.; Hiskia, A. Photocatalytic Degradation of Water Taste and Odour Compounds in the Presence of Polyoxometalates and TiO2: Intermediates and Degradation Pathways. *J. Photochem. Photobiol., A* **2014**, *286*, 1−9.

(17) Lauinger, S. M.; Sumliner, J. M.; Yin, Q.; Xu, Z.; Liang, G.; Glass, E. N.; Lian, T.; Hill, C. L. High Stability of Immobilized Polyoxometalates on TiO2 Nanoparticles and Nanoporous Films for Robust, Light-Induced Water Oxidation. *Chem. Mater.* **2015**, *27*, 5886−5891.

(18) Gu, J.; Chen, W.; Shan, G. G.; Li, G.; Sun, C.; Wang, X. L.; Su, Z. The Roles of Polyoxometalates in Photocatalytic Reduction of Carbon Dioxide. *Mater. Today Energy* **2021**, *21*, 100760.

(19) Lan, J.; Wang, Y.; Huang, B.; Xiao, Z.; Wu, P. Application of Polyoxometalates in Photocatalytic Degradation of Organic Pollutants. *Nanoscale Adv.* **2021**, *3*, 4646−4658.

(20) Lai, S. Y.; Ng, K. H.; Cheng, C. K.; Nur, H.; Nurhadi, M.; Arumugam, M. Photocatalytic Remediation of Organic Waste over Keggin-Based Polyoxometalate Materials: A Review. *Chemosphere* **2021**, *263*, 128244.

(21) Knoth, W. H.; Domaille, P. J.; Roe, D. C. Halometal derivatives of W12PO403- and related tungsten-183 NMR studies. *Inorg. Chem.* **1983**, *22*, 198−201.

(22) Fan, X. Y.; Guo, H.; Lv, J. H.; Yu, K.; Su, Z. H.; Wang, L.; Wang, C. M.; Zhou, B. B. Efficient and Robust Photocatalysts Based on {P2W18} Modified by an Ag Complex. *Dalton Trans.* **2018**, *47*, 4273−4281.

(23) Wu, P.; Wang, Y.; Huang, B.; Xiao, Z. Anderson-Type Polyoxometalates: From Structures to Functions. *Nanoscale* **2021**, *13*, 7119−7133.

(24) Qin, L.; Ren, R.; Huang, X.; Xu, X.; Shi, H.; Huai, R.; Song, N.; Yang, L.; Wang, S.; Zhang, D.; Zhou, Z. Photocatalytic Activity of an Anderson-Type Polyoxometalate with Mixed Copper(I)/Copper(II) Ions for Visible-Light Enhancing Heterogeneous Catalysis. *J. Solid State Chem.* **2022**, *310*, 123052.

(25) Wang, X.; Chang, Z.; Lin, H.; Tian, A.; Liu, G.; Zhang, J. Assembly and Photocatalysis of Two Novel 3D Anderson-Type Polyoxometalate-Based Metal−Organic Frameworks Constructed from Isomeric Bis(Pyridylformyl)Piperazine Ligands. *Dalton Trans.* **2014**, *43*, 12272−12278.

(26) Sivakumar, R.; Thomas, J.; Yoon, M. Polyoxometalate-Based Molecular/Nano Composites: Advances in Environmental Remediation by Photocatalysis and Biomimetic Approaches to Solar Energy Conversion. *J. Photochem. Photobiol., C* **2012**, *13*, 277−298.

(27) Diaz-Uribe, C. E.; Rodríguez, A.; Utria, D.; Vallejo, W.; Puello, E.; Zarate, X.; Schott, E. Photocatalytic Degradation of Methylene Blue by the Anderson-Type Polyoxomolybdates/TiO2 Thin Films. *Polyhedron* **2018**, *149*, 163−170.

(28) Sanguino, A.; Diaz-Uribe, C.; Duran, F.; Vallejo, W.; Guzman, L.; Ruiz, D.; Puello, E.; Quiñones, C.; Schott, E.; Zarate, X. Photocatalytic Degradation of Methylene Blue under Visible Light Using TiO2 Thin Films Impregnated with Porphyrin and Anderson-Type Polyoxometalates (Cu and Zn). *Catal* **2022**, *12*, 1169.

(29) Lee, U.; Joo, H.-C.; Kwon, J.-S. Tetraammonium Hexahydrogen Hexamolybdonickelate(II) Tetrahydrate, (NH 4) 4 [H 6 NiMo 6 O 24]·4H 2 O. *Acta Crystallogr., Sect. E: Struct. Rep. Online* **2002**, *58*, i6−i8.

(30) Kontos, A. I.; Kontos, A. G.; Tsoukleris, D. S.; Bernard, M.-C.; Spyrellis, N.; Falaras, P. Nanostructured TiO2 Films for DSSCS Prepared by Combining Doctor-Blade and Sol−Gel Techniques. *J. Mater. Process. Technol.* **2008**, *196*, 243−248.

(31) Quiñones, C.; Ayala, J.; Vallejo, W. Methylene blue photoelectrodegradation under UV irradiation on Au/Pd-modified TiO2 films. *Appl. Surf. Sci.* **2010**, *257*, 367−371.

(32) Konstantinou, I. K.; Albanis, T. A. TiO2-assisted photocatalytic degradation of azo dyes in aqueous solution: kinetic and mechanistic investigations. *Appl. Catal., B* **2004**, *49*, 1−14.

(33) te Velde, G.; Bickelhaupt, F. M.; Baerends, E. J.; Fonseca Guerra, C.; van Gisbergen, S. J. A.; Snijders, J. G.; Ziegler, T. Chemistry with ADF. *J. Comput. Chem.* **2001**, *22*, 931−967.

(34) Van Lenthe, E.; Baerends, E. J.; Snijders, J. G. Relativistic Total Energy Using Regular Approximations. *J. Chem. Phys.* **1994**, *101*, 9783−9792.

(35) Snijders, J. G.; Vernooijs, P.; Baerends, E. J. Roothaan-Hartree-Fock-Slater Atomic Wave Functions: Single-Zeta, Double-Zeta, and Extended Slater-Type Basis Sets for 87Fr-103Lr. *At. Data Nucl. Data Tables* **1981**, *26*, 483−509.

https://doi.org/10.1021/acsomega.3c02657
ACS Omega 2023, 8, 27284−27292

(36) Laskowski, R.; Blaha, P.; Tran, F. Assessment of DFT Functionals with NMR Chemical Shifts. *Phys. Rev. B: Condens. Matter Mater. Phys.* **2013**, *87*, 195130.
(37) Toure, O.; Lebert, A.; Dussap, C. G. Extension of the COSMO-RS-PDHS Model to the Prediction of Activity Coefficients in Concentrated {water-Electrolyte} and {water-Polyol} Solutions. *Fluid Phase Equilib.* **2016**, *424*, 90−104.
(38) Ziegler, T.; Rauk, A. A theoretical study of the ethylene-metal bond in complexes between copper(1+), silver(1+), gold(1+), platinum(0) or platinum(2+) and ethylene, based on the Hartree-Fock-Slater transition-state method. *Inorg. Chem.* **1979**, *18*, 1558−1565.
(39) Ziegler, T.; Rauk, A. On the Calculation of Bonding Energies by the Hartree Fock Slater Method. *Theor. Chim. acta* **1977**, *46*, 1−10.
(40) Schott, E.; Zárate, X.; Arratia-Pérez, R. Relativistic Scalar and Spin−Orbit Density Functional Calculations of the Electronic Structure, NICS Index and ELF Function of the [Re2(CO)8(μ-BiPh)2] and [Re2(CO)8(μ-BiPh2)2] Clusters. *Polyhedron* **2011**, *30*, 846−850.
(41) Kamarulzaman, N. H.; Salleh, H.; Dagang, A. N.; Mohd Ghazali, M. S.; Ishak, N.; Ahmad, Z. Optimization of Titanium Dioxide Layer Fabrication Using Doctor Blade Method in Improving Efficiency of Hybrid Solar Cells. *J. Phys.: Conf. Ser.* **2020**, *1535*, 012025.
(42) Janarthanan, B.; Thirunavukkarasu, C.; Maruthamuthu, S.; Manthrammel, M. A.; Shkir, M.; AlFaify, S.; Selvakumar, M.; Reddy, V. R. M.; Park, C. Basic Deposition Methods of Thin Films. *J. Mol. Struct.* **2021**, *1241*, 130606.
(43) Ramos-Hernández, R.; Calvo, F. D.; Pérez-Gutiérrez, E.; Percino, M. J. Large Area Small-Molecule Thin Films Deposited by the Doctor Blade Technique Implemented with Computer Numerical Control Machine. *Thin Solid Films* **2023**, *771*, 139787.
(44) Chonsut, T.; Rangkasikorn, A.; Wirunchit, S.; Kaewprajak, A.; Kumnorkaew, P.; Kayunkid, N.; Nukeaw, J. Rapid Convective Deposition; an Alternative Method to Prepare Organic Thin Film in Scale of Nanometer. *Mater. Today: Proc.* **2017**, *4*, 6134−6139.
(45) Sun, Z.; Zhao, M.; Li, F.; Wang, T.; Xu, L. Nanocomposite Film of TiO2 Nanotube and Polyoxometalate towards Photocatalytic Degradation of Nitrobenzene. *Mater. Res. Bull.* **2014**, *60*, 524−529.
(46) Yang, Y.; Guo, Y.; Hu, C.; Jiang, C.; Wang, E. Synergistic Effect of Keggin-Type [Xn+W11O39](12−n)− and TiO2 in Macroporous Hybrid Materials [Xn+W11O39](12−n)−−TiO2 for the Photocatalytic Degradation of Textile Dyes. *J. Mater. Chem.* **2003**, *13*, 1686−1694.
(47) Li, K.; Guo, Y.; Ma, F.; Li, H.; Chen, L.; Guo, Y. Design of Ordered Mesoporous H3PW12O40-Titania Materials and Their Photocatalytic Activity to Dye Methyl Orange Degradation. *Catal. Commun.* **2010**, *11*, 839−843.
(48) Simmons, E. L. Relation of the Diffuse Reflectance Remission Function to the Fundamental Optical Parameters. *Opt. Acta Int. J. Opt.* **1972**, *19*, 845−851.
(49) Madhusudan Reddy, K.; Manorama, S. V.; Ramachandra Reddy, A. Bandgap Studies on Anatase Titanium Dioxide Nanoparticles. *Mater. Chem. Phys.* **2003**, *78*, 239−245.
(50) Sahoo, T. R.; Prelot, B. Adsorption Processes for the Removal of Contaminants from Wastewater: The Perspective Role of Nanomaterials and Nanotechnology. *Nanomater. Detect. Removal Wastewater Pollut.* **2020**, 161−222.
(51) Adamson, A. W.; Gast, A. P.; Alice, P. *Physical Chemistry of Surfaces*; Interscience publishers New York, 1997; p 784.
(52) Ayawei, N.; Ebelegi, A. N.; Wankasi, D. Modelling and Interpretation of Adsorption Isotherms. *J. Chem.* **2017**, *2017*, 1−11.
(53) Wang, J. L.; Xu, L. J. Advanced Oxidation Processes for Wastewater Treatment: Formation of Hydroxyl Radical and Application. *Crit. Rev. Environ. Sci. Technol.* **2012**, *42*, 251−325.
(54) Diaz-Uribe, C.; Duran, F.; Vallejo, W.; Puello, E.; Zarate, X.; Schott, E. Photocatalytic Study of TiO2 Thin Films Modified with Anderson-Type Polyoxometalates (Cr, Co and Ni): Experimental and DFT Study. *Polyhedron* **2023**, *231*, 116253.
(55) Hua, Y.; Wang, C.; Liu, J.; Wang, B.; Liu, X.; Wu, C.; Liu, X. Visible Photocatalytic Degradation of Rhodamine B Using Fe(III)-Substituted Phosphotungstic Heteropolyanion. *J. Mol. Catal. A: Chem.* **2012**, *365*, 8−14.
(56) Chen, X.; Wu, H.; Shi, X.; Wu, L. Polyoxometalate-Based Frameworks for Photocatalysis and Photothermal Catalysis. *Nanoscale* **2023**, *15*, 9242−9255.
(57) Li, L.; Yang, Y.; Fan, R.; Liu, J.; Jiang, Y.; Yang, B.; Cao, W. Decatungstate Acid Improves the Photo-Induced Electron Lifetime and Retards the Recombination in Dye Sensitized Solar Cells. *Dalton Trans.* **2016**, *45*, 14940−14947.

https://doi.org/10.1021/acsomega.3c02657
ACS Omega 2023, 8, 27284−27292